SATELLITE PASSIVE MICROWAVE MEASUREMENTS OF SEA ICE

C. L. Parkinson, NASA Goddard Space Flight Center, Greenbelt, MD, USA

Introduction

Satellite passive-microwave measurements of sea ice have provided global or near-global sea ice data for most of the period since the launch of the Nimbus 5 satellite in December 1972, and have done so with horizontal resolutions on the order of 25–50 km and a frequency of every few days. These data have been used to calculate sea ice concentrations (percent areal coverages), sea ice extents, the length of the sea ice season, sea ice temperatures, and sea ice velocities, and to determine the timing of the seasonal onset of melt as well as aspects of the ice-type composition of the sea ice cover. In each case, the calculations are based on the microwave emission characteristics of sea ice and the important contrasts between the microwave emissions of sea ice and those of the surrounding liquid-water medium.

Background on Satellite Passive-Microwave Sensing of Sea Ice

Rationale

Sea ice is a vital component of the climate of the polar regions, insulating the oceans from the atmosphere, reflecting most of the solar radiation incident on it, transporting cold, relatively fresh water equatorward, and at times precipitating overturning in the ocean and even bottom water formation through its rejection of salt to the underlying water. Furthermore, sea ice spreads over vast distances, globally covering an area approximately the size of North America at any given time, and it is highly dynamic, experiencing a prominent annual cycle in both polar regions and many short-term fluctuations as it is moved by winds and waves, melted by solar radiation, and augmented by additional freezing. It is a major player in and indicator of the polar climate state, and consequently it is highly desirable to monitor the sea ice cover on a routine basis. In view of the vast areal coverage of the ice and the harsh polar conditions, the only feasible means of obtaining routine monitoring is through satellite observations. Visible, infrared, active-microwave, and passive-microwave satellite instruments are all proving useful for examining the sea ice cover, with the passive-microwave instruments providing the longest record of near complete sea ice monitoring on a daily or near daily basis.

Theory

The tremendous value of satellite passive-microwave measurements for sea ice studies results from the combination of the following factors:

1. Microwave emissions of sea ice differ noticeably from those of sea water, making sea ice generally readily distinguishable from liquid water on the basis of the amount of microwave radiation received by the satellite instrument. For example, **Figure 1** presents color-coded images of the data from one channel on a satellite passive-microwave instrument, presented in units (termed 'brightness temperatures') indicative of the intensity of emitted microwave radiation at that channel's frequency, 19.4 GHz. The ice edge, highlighted by the dashed white curve, is clearly identifiable from the brightness temperatures, with open-ocean values of 172–198 K outside the ice edge and sea ice values considerably higher, predominantly greater than 230 K, within the ice edge.

2. The microwave radiation received by earth-orbiting satellites derives almost exclusively from the earth system. Hence, microwave sensing does not require sunlight, and the data can be collected irrespective of the level of daylight or darkness. This is a major advantage in the high polar latitudes, where darkness lasts for months at a time, centered on the winter solstice.

3. Many of the microwave data are largely unaffected by atmospheric conditions, including the presence or absence of clouds. Storm systems can produce atmospheric interference, but the microwave signal from the ice–ocean surface can pass through most nonprecipitating clouds essentially unhindered. Hence, microwave sensing of the surface does not require cloud-free conditions.

4. Satellite passive-microwave instruments can obtain a global picture of the sea ice cover at least every few days with a resolution of 50 km or better, providing reasonable spatial resolution

and extremely good temporal resolution for most large-scale or climate-related studies.

Satellite Passive-Microwave Instruments

The first major satellite passive-microwave imager was the Electrically Scanning Microwave Radiometer (ESMR) launched on the Nimbus 5 satellite of the US National Aeronautics and Space Administration (NASA) in December 1972, preceded by a nonscanning passive-microwave radiometer launched on the Russian Cosmos satellite in September 1968. The ESMR was a single-channel instrument recording radiation at a wavelength of 1.55 cm and corresponding frequency of 19.35 GHz. It collected good-quality data for much of the 4-year period from January 1973 through December 1976, although with some major data gaps, including one that lasted for 3 months, from June through August 1975. Being a single-channel instrument, it did not allow some of the more advanced studies that have been done with subsequent instruments, but its flight was a highly successful proof-of-concept mission, establishing the value of satellite passive-microwave technology for observing the global sea ice cover. The ESMR data were used extensively in the determination and analysis of sea ice conditions in both the Arctic and the Antarctic over the four years 1973–1976. Emphasis centered on the determination of ice concentrations (percent areal coverages of ice) and, based on the ice concentration results, the calculation of ice extents (integrated areas of all grid elements with ice concentration $\geq 15\%$).

The Nimbus 5 ESMR was followed by a less successful ESMR on the Nimbus 6 satellite and then by the more advanced 10-channel Scanning Multichannel Microwave Radiometer (SMMR) on board NASA's Nimbus 7 satellite and a sequence of 7-channel Special Sensor Microwave Imagers (SSMIs) on board satellites of the United States Defense Meteorological Satellite Program (DMSP). The Nimbus 7 was launched in late October 1978, and the SMMR on board it was operational through mid-August 1987. The first of the DMSP SSMIs was operational as of early July 1987, providing welcome data overlap with the Nimbus 7 SMMR and thereby allowing intercalibration of the SMMR and SSMI data sets. SSMIs continue to operate into the twenty-first century. There was also a SMMR on board the short-lived Seasat satellite in 1978; and there was a 2-channel Microwave Scanning Radiometer (MSR) on board the Japanese Marine Observation Satellites starting in February 1987. Each of these successor satellite passive-microwave instruments, after the ESMR, has been multichannel, allowing both an improved accuracy in the ice concentration derivations and the calculation of additional sea ice variables, including ice temperature and the concentrations of separate ice types.

The Japanese have developed an Advanced Microwave Scanning Radiometer (AMSR) for the Earth Observing System's Aqua satellite (formerly named the PM-1 satellite), scheduled for launch by NASA in December 2001, and for the Advanced Earth Observing Satellite II, scheduled for launch by the Japanese National Space Development Agency in February 2002. The AMSR will allow sea ice measurements at a higher spatial resolution (12–25 km) than is currently available with the SSMI instruments (25–50 km resolution for the major derived sea ice products).

Sea Ice Determinations from Satellite Passive-Microwave Data

Sea Ice Concentrations

Ice concentration is among the most fundamental and important parameters for describing the sea ice cover. Defined as the percent areal coverage of ice, it is directly critical to how much impact the ice cover has on restricting exchanges between the ocean and atmosphere and on reflecting incoming solar radiation. Ice concentration is calculated at each ocean grid element, for whichever grid is being used to map or otherwise display the derived satellite products. A map of ice concentrations presents the areal distribution of the ice cover, to the resolution of the grid. In cases where ice thickness data are also available, the combination of ice concentration and ice thickness allows the calculation of ice volume.

With a single channel of microwave data, taken at a radiative frequency and polarization combination that provides a clear distinction between ice and water, approximate sea ice concentrations can be calculated by assuming a uniform radiative brightness temperature TB_w for water and a uniform radiative brightness temperature TB_I for ice, with both brightness temperatures being appropriate for the values received at the altitude of the satellite, i.e., incorporating an atmospheric contribution. Assuming no other surface types within the field of view, the observed brightness temperature TB is given by eqn [1].

$$TB = C_w TB_w + C_I TB_I \qquad [1]$$

C_w is the percent areal coverage of water and C_I is the ice concentration. With only the two surface types, $C_w + C_I = 1$, and eqn [1] can be expressed as eqn [2].

$$TB = (1 - C_I)TB_w + C_I TB_I \qquad [2]$$

This is readily solved for the ice concentration (eqn [3]).

$$C_I = \frac{TB - TB_w}{TB_I - TB_w} \qquad [3]$$

Equation [3] is the standard equation used for the calculation of ice concentrations from a single channel of microwave data, such as the data from the ESMR instrument. A major limitation of the formulation is that the polar ice cover is not uniform in its microwave emission, so that the assumption of a uniform TB_I for all sea ice is only a rough approximation, far less justified than the assumption of a uniform TB_w for sea water, although that also is an approximation.

Multichannel instruments allow more sophisticated, and generally more accurate, calculation of the ice concentrations. They additionally allow many options as to how these calculations can be done. To illustrate the options, two algorithms will be described, both of which assume two distinct ice types, thereby advancing over the assumption of a single ice type made in eqns [1]–[3], especially for the many instances in which two ice types dominate the sea ice cover. Assume then that the field of view contains only water and two ice types, type 1 ice and type 2 ice (see later for more on ice types), and that the three surface types have identifiable brightness temperatures, TB_w, TB_{I1}, and TB_{I2}, respectively. Labeling the concentrations of the two ice types as C_{I1} and C_{I2}, respectively, the percent coverage of water is $1 - C_{I1} - C_{I2}$, and the integrated observed brightness temperature is given by eqn [4].

$$TB = (1 - C_{I1} - C_{I2})TB_w + C_{I1}TB_{I1} + C_{I2}TB_{I2} \qquad [4]$$

With two channels of information, as long as appropriate values for TB_w, TB_{I1}, and TB_{I2} are known for each of the two channels, eqn [4] can be used individually for each channel, yielding two linear equations in the two unknowns C_{I1} and C_{I2}. These equations are immediately solvable for C_{I1} and C_{I2}, and the total ice concentration C_I is then given by eqn [5].

$$C_I = C_{I1} + C_{I2} \qquad [5]$$

Although the scheme described in the preceding paragraph is a marked advance over the use of a single-channel calculation (eqn [3]), most algorithms for sea ice concentrations from multichannel data make use of additional channels and concepts to improve further the ice concentration accuracies. A widely used algorithm (termed the NASA Team algorithm) for the SMMR data employs three of the ten SMMR channels, those recording horizontally polarized radiation at a frequency of 18 GHz and vertically polarized radiation at frequencies of 18 GHz and 37 GHz. The algorithm is based on both the polarization ratio (PR) between the 18 GHz vertically polarized data (abbreviated 18 V) and the 18 GHz horizontally polarized data (18 H) and the spectral gradient ratio (GR) between the 37 GHz vertically polarized data (37 V) and the 18 V data. PR and GR are defined in eqns [6] and [7].

$$PR = \frac{TB(18V) - TB(18H)}{TB(18V) + TB(18H)} \qquad [6]$$

$$GR = \frac{TB(37V) - TB(18V)}{TB(37V) + TB(18V)} \qquad [7]$$

Substituting into eqns [6] and [7] expanded forms of $TB(18\,V)$, $TB(18\,H)$, and $TB(37\,V)$ obtained from eqn [4], the result yields equations for PR and GR in the two unknowns C_{I1} and C_{I2}. Solving for C_{I1} and C_{I2} yields two algebraically messy but computationally straightforward equations for C_{I1} and C_{I2} based on PR, GR, and numerical coefficients determined exclusively from the brightness temperature values assigned to water, type 1 ice, and type 2 ice for each of the three channels (these assigned values are termed 'tie points' and are determined empirically). These are the equations that are then used for the calculation of the concentrations of type 1 and type 2 ice once the observations are made and are used to calculate PR and GR from eqns [6] and [7]. The total ice concentration C_I is then obtained from eqn [5]. The use of PR and GR in this formulation reduces the impact of ice temperature variations on the ice concentration calculations. This algorithm is complemented by a weather filter that sets to 0 all ice concentrations at any time and location with a GR value exceeding 0.07. The weather filter eliminates many of the erroneous calculations of sea ice presence arising from the influence of storm systems on the microwave data.

For the SSMI data, the same basic NASA Team algorithm is used, although 18 V and 18 H in
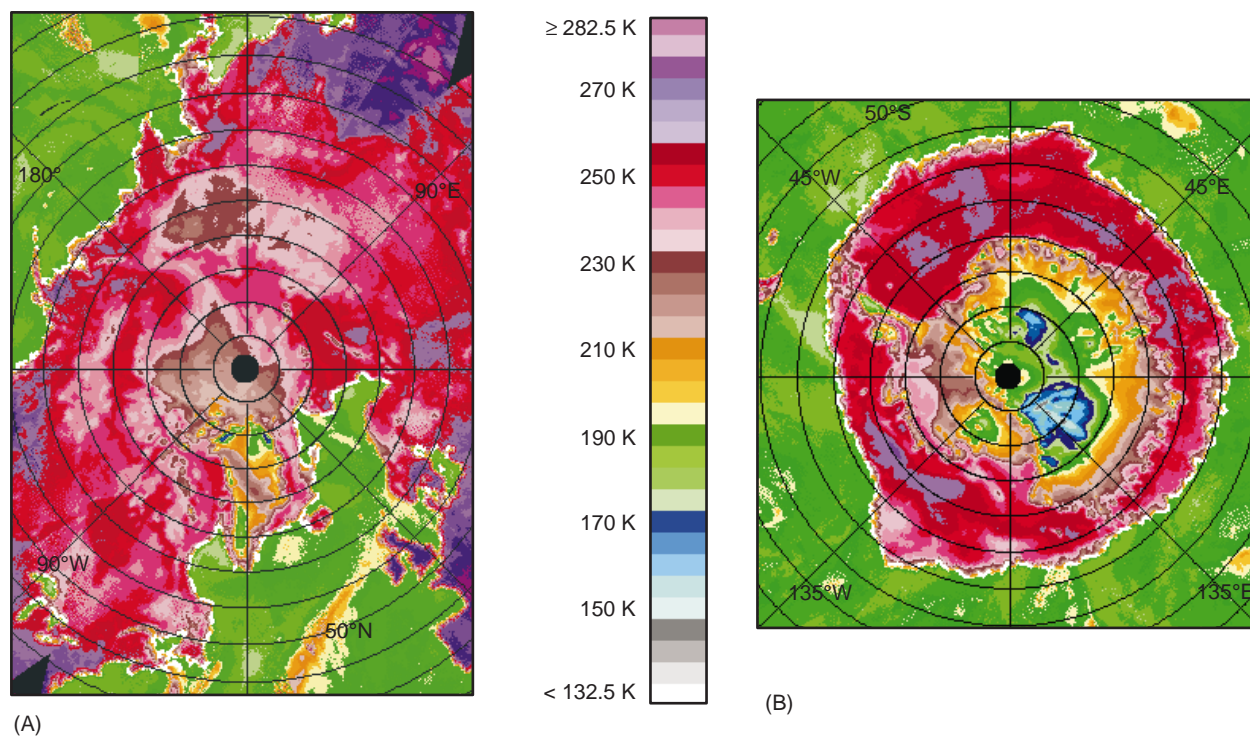
Figure 1   Late winter brightness temperature images of 19.4 GHz vertically polarized (19.4 V) data from the Defense Meteorological Satellite Program's Special Sensor Microwave Imager (SSMI) for (A) the north polar region on 15 March 1998, and (B) the south polar region on 15 September 1998, showing near-maximum sea ice coverage in each hemisphere. The dashed white curve has been added to indicate the location of the sea ice edge. Black signifies areas of no data; the absence of data poleward of 87.6° latitude results from the satellite's near-polar orbit and is consistent throughout the data set.

eqns [6] and [7] are replaced by 19.4 V and 19.4 H, reflecting the placement on the SSMI of channels at a frequency of 19.4 GHz rather than the 18 GHz channels on the SMMR. Also, because the data from the 19.4 GHz channels tend to be more contaminated by water vapor absorption/emission and other weather effects than the 18 GHz data, the weather filter for the SSMI calculations incorporates a threshold level for the gradient ratio calculated from the 22.2 GHz vertically polarized data and 19.4 V data as well as a threshold for the gradient ratio calculated from the 37 V and 19.4 V data. To illustrate the results of this ice concentration algorithm, **Figure 2** presents the derived sea ice concentrations for March 15, 1998 in the Northern Hemisphere and for September 15, 1998 in the Southern Hemisphere, the same dates as used in **Figure 1**.

As mentioned, there are several alternative ice concentration algorithms in use. Contrasts from the NASA Team algorithm just described include: use of different microwave channels; use of regional tie points rather than hemispherically applicable tie points; use of cluster analysis on brightness temperature data, without *PR* and *GR* formulations; use of

iterative techniques whereby an initial ice concentration calculation leads to refined atmospheric temperatures and opacities, which in turn lead to refined ice concentrations; use of iterative techniques involving surface temperature, atmospheric water vapor, cloud liquid water content, and wind speed; and use of a Kalman filtering technique in conjunction with an ice model. The various techniques tend to obtain very close overall distributions of where the sea ice is located, although sometimes with noticeable differences (up to 20%, and on occasion even higher) in the individual, local ice concentrations. The differences can often be markedly reduced by adjustment of tunable parameters, such as the algorithm tie points, in one or both of the algorithms being compared. However, the lack of adequate ground data often makes it difficult to know which tuning is most appropriate or which algorithm is yielding the better results.

Sea Ice Extents

Sea ice extent is defined as the area of coverage of sea ice of at least some set percentage ice concentration, with the set percentage most frequently being
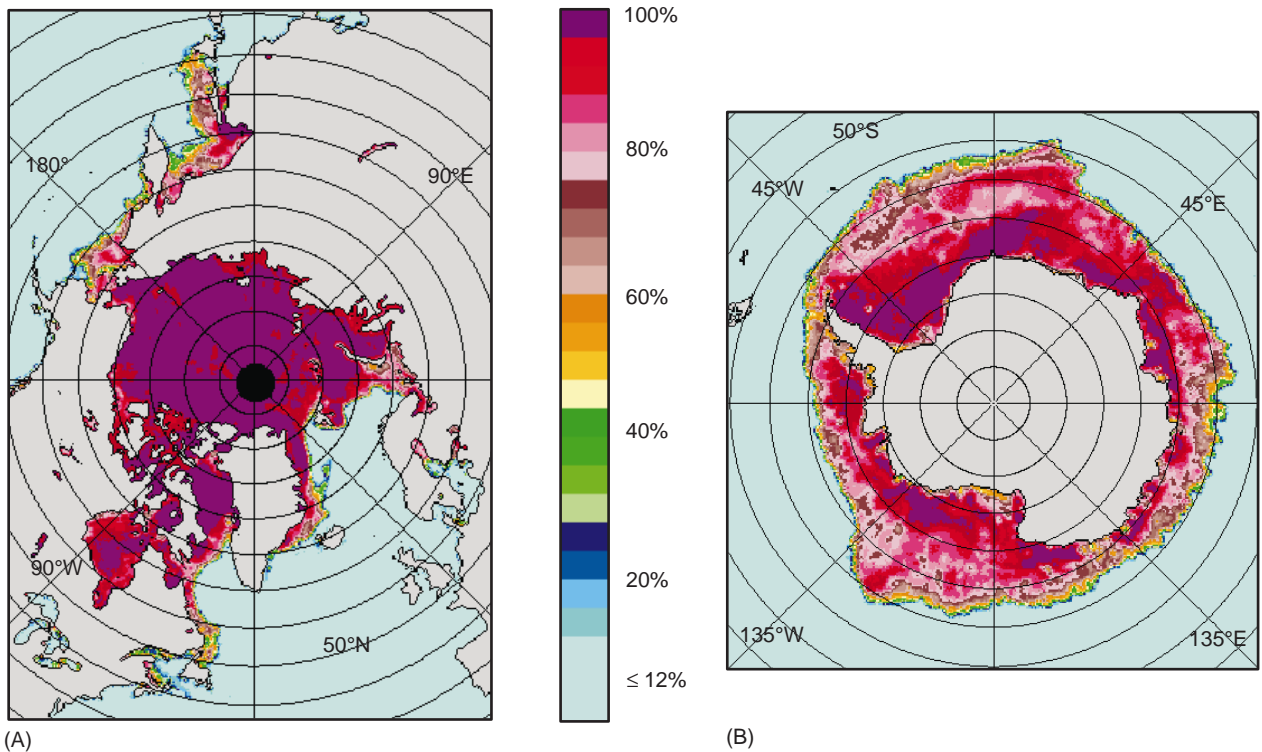
Figure 2 North and south polar sea ice concentration images for (A) 15 March 1998 and (B) 15 September 1998, respectively. The ice concentrations are derived from the data of the DMSP SSMI, including the 19.4 V data depicted in **Figure 1**.

15%. Sea ice extents are readily calculated from sea ice concentration maps by adding the areas of all grid elements in the region of interest having a calculated ice concentration of at least the predetermined cutoff (generally 15%). Ice extents are now regularly calculated from satellite passive-microwave data for the north polar region as a whole, for the south polar region as a whole, and for each of many subregions within the two polar domains.

A major early result in the use of satellite passive-microwave data was the detailed determination of the seasonal cycle of ice extents in each hemisphere. The Southern Ocean ice extents vary from about $2-4 \times 10^6$ km^2 in February to about $17-20 \times 10^6$ km^2 in September; the north polar ice extents vary from about $6-8 \times 10^6$ km^2 in September to about $14-16 \times 10^6$ km^2 in March. The ranges reflect the level of interannual variability observed from the satellite record over the course of the 1970s through the 1990s.

As the data sets lengthened, a major goal became the determination of trends in the ice extents and placement of these trends in the context of other climate variables and climate change. Because of the lack of a period of data overlap between the ESMR and the SMMR, matching of the ice extents derived

from the ESMR data to those derived from the SMMR and SSMI data has been difficult and uncertain. Consequently, published results regarding trends found from the latter two data sets generally do not include the ESMR data. However, trends have been calculated for the combined SMMR/SSMI data set, and these calculations have been done for the data set as a whole, for individual seasons and months, and for individual regions. For the data set as a whole, the SMMR/SSMI record from late 1978 until the late 1990s indicates an overall decrease in Arctic ice extents of about 2–3% per decade and an overall increase in Antarctic ice extents of about 1–2% per decade. In both hemispheres, the trends are nonuniform with time and individual regions within the hemisphere display percent per decade trends of higher magnitude, some with positive signs and some with negative signs. These concepts are illustrated in **Figure 3A** with 20-year March time series for the Northern Hemisphere and two regions within the Northern Hemisphere and in **Figure 3B** with 20-year September time series for the Southern Hemisphere and two seas within the Southern Hemisphere. March and September are generally the months with the most sea ice coverage in the respective hemispheres.
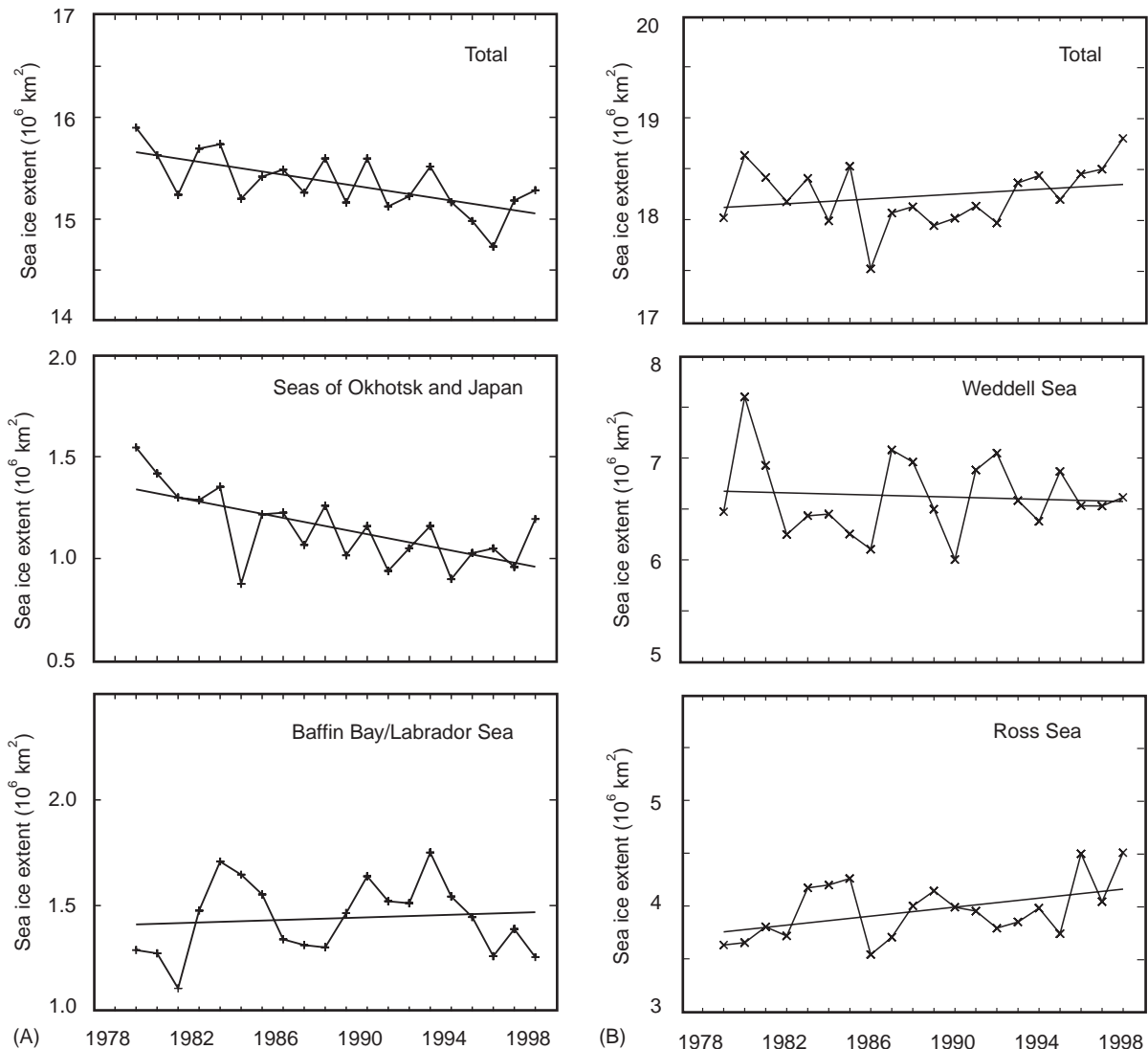
Figure 3 (A) Time series of monthly average 1979–1998 March sea ice extents for the Northern Hemisphere and two regions within the Northern Hemisphere. (B) Time series of monthly average 1979–1998 September sea ice extents for the Southern Hemisphere and two regions within the Southern Hemisphere. All ice extents are derived from the Nimbus 7 SMMR and DMSP SSMI data. The trend lines have slopes of $-31700 \, \mathrm{km^2 \, y^{-1}}$ (-2.0% per decade) for the Northern Hemisphere total; $-20000 \, \mathrm{km^2 \, y^{-1}}$ (-14.9% per decade) for the Seas of Okhotsk and Japan; $3100 \, \mathrm{km^2 \, y^{-1}}$ (2.2% per decade) for Baffin Bay/Labrador Sea; $11900 \, \mathrm{km^2 \, y^{-1}}$ (0.7% per decade) for the Southern Hemisphere total; $-5300 \, \mathrm{km^2 \, y^{-1}}$ (-0.8% per decade) for the Weddell Sea; and $21300 \, \mathrm{km^2 \, y^{-1}}$ (5.7% per decade) for the Ross Sea.

Sea Ice Types

The sea ice cover in both polar regions is a mixture of various types of ice, ranging from individual ice crystals to coherent ice floes several kilometers across. Common ice types include frazil ice (fine spicules of ice suspended in water); grease ice (a soupy layer of ice that looks like grease from a distance); slush ice (a viscous mass formed from a mixture of water and snow); nilas (a thin elastic sheet of ice 0.01–0.1 m thick); pancake ice (small, roughly circular pieces of ice, 0.3–3 m across and up to 0.1 m thick); first-year ice (ice at least 0.3 m thick that has not yet undergone a summer melt period); and multiyear ice (ice that has survived a summer melt).

Because different ice types have different microwave emission characteristics, once these differences are understood, appropriate satellite passive-microwave data can be used to distinguish ice types. The ice types most frequently distinguished with such data are first-year ice and multiyear ice in the
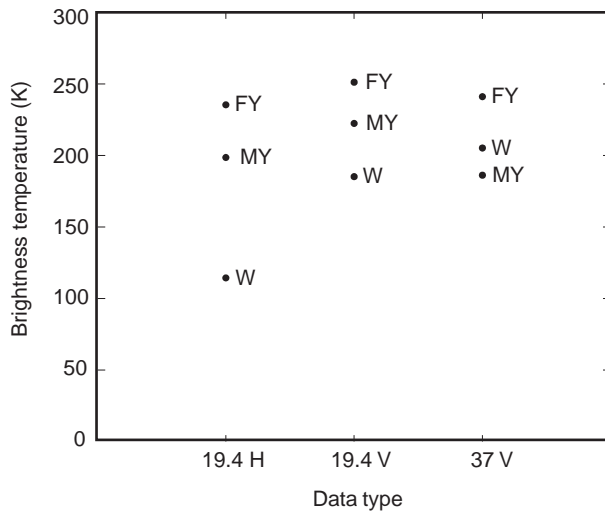
Figure 4 Brightness temperatures of first-year ice (FY), multi-year ice (MY), and liquid water (W) at three channels of SSMI data from the DMSP F13 satellite. These are the values used as tie points for the Arctic calculations in the NASA Team algorithm described in the text. (Data from Cavalieri *et al.* (1999).)

Arctic Ocean. In fact, the NASA Team algorithm described earlier was initially developed specifically for first-year and multiyear ice, with the resulting calculations yielding the concentrations, C_{I1} and C_{I2}, of those two ice types. First-year and multiyear ice are distinguishable in their microwave signals because the summer melt process drains down through the ice some of its salt content, reducing the salinity of the upper layers of the ice and thereby changing the microwave emissions; these changes are dependent on the frequency and polarization of the radiation. To illustrate the differences, **Figure 4** presents a plot of the tie points used by the NASA Team algorithm in the Arctic for the three SSMI channels used to calculate ice concentrations prior to the application of the weather filter. The plot shows that while the transition from first-year to multiyear ice lowers the brightness temperatures for each of the three channels, the reduction is greatest for the 37 V data and least for the 19.4 V data. Examination of **Figure 4** further reveals that the polarization PR (eqn [6], revised for 19.4 GHz rather than 18 GHz data) increases from first-year to multiyear ice, though it remains well below the polarization of water, and that the gradient ratio GR (eqn [7], revised for 19.4 GHz data) is positive for water, slightly negative for first-year ice, and considerably more negative for multiyear ice. The differences allow the sorting out, either through the calculation of C_{I1} and C_{I2} as described or through alternative algorithms, of the first-year ice and multiyear ice percentages in the satellite field of view.

Other Sea Ice Variables: Season Length, Temperature, Melt, Velocity

Although sea ice concentrations, extents, and, to a lesser degree, types have been the sea ice variables most widely calculated and used from satellite passive-microwave data, several additional variables have also been obtained from these data, including the length of the sea ice season, sea ice temperature, sea ice melt, and sea ice velocity. The length of the sea ice season for any particular year is calculated directly from that year's daily maps of sea ice concentrations, by counting, at each grid element, the number of days with ice coverage of at least some predetermined (generally 15% or 30%) ice concentration. Trends in the length of the sea ice season from the late 1970s to the 1990s show coherent spatial patterns in both hemispheres, with a predominance of negative values (shortening of the sea ice season) in the Northern Hemisphere and a predominance of positive values in the Southern Hemisphere, consistent with the respective hemispheric trends in sea ice extents.

The passive-microwave-based ice temperature calculations generally depend on the calculated sea ice concentrations, empirically determined ice emissivities, a weighting of the water and ice temperatures within the field of view, and varying levels of sophistication in incorporating effects of the polar atmosphere and the presence of multiple ice types. The derived temperature is not the surface temperature but the temperature of the radiating portion of the ice, for whichever radiative frequency is being used. The ice temperature fields derived from passive-microwave data complement those derived from satellite infrared data, which have the advantages of having finer spatial resolution and more nearly approaching surface temperatures but the disadvantage of greater contamination by clouds. The passive-microwave and infrared data are occasionally used together, iteratively, for an enhanced ice temperature product.

The seasonal onset of melt on the sea ice and its overlying snow cover generally produces marked changes in microwave emissions, first increasing the emissions as liquid water emerges in the snow, then decreasing the emissions once the snow has melted and meltwater ponds cover the ice. Because of the emission changes, these events on the ice surface frequently become detectable through time series of the satellite passive-microwave data. The onset of melt in particular can often be identified, and hence yearly maps can be created of the dates of melt onset. Melt ponds, however, present greater difficulties, as they can have similar microwave emissions

to those of the water in open spaces between ice floes, so that a field of heavily melt-ponded ice can easily be confused in the microwave data with a field of low-concentration ice. The ambiguities can be reduced through analysis of the passive-microwave time series and comparisons with active-microwave, visible, and infrared data.

The calculation of sea ice velocities from satellite data has in general relied upon data with fine enough resolution to distinguish individual ice floes, such as visible data and active-microwave data rather than the much coarser resolution passive-microwave data. However, in the 1990s several groups devised methods of determining ice velocity fields from passive-microwave data, some using techniques based on cross-correlation of brightness temperature fields and others using wavelet analysis. These techniques have yielded ice velocity maps on individual dates for the entire north and south polar sea ice covers. Comparisons with buoy and other data have been quite encouraging regarding the potential of using the satellite data for long-term records and monitoring of ice motions.

Looking Toward the Future

Monitoring of the polar sea ice covers through satellite passive-microwave technology is ongoing with the operational United States SSMI instruments and should be further enhanced with the Japanese AMSR instruments scheduled for launch in 2001 and 2002. The resulting lengthening sea ice records provide an improved basis with which scientists can examine trends in the sea ice cover and interactions between the sea ice and other elements of the climate system. For instance, the lengthened records will be essential to answering many of the questions raised concerning whether the negative overall trends found in Arctic sea ice extents for the first two decades of the SMMR/SSMI record will continue and how these trends relate to temperature trends, in particular to possible climate warming, and to oscillations within the climate system, in particular the North Atlantic Oscillation, the Arctic Oscillation, and the Southern Oscillation. In addition to covering a longer period, other expected improvements in the satellite passive-microwave record of sea ice include further algorithm developments, following additional analyses on the microwave properties of sea ice and liquid water. Such analyses are likely to lead both to improved algorithms for the variables already examined and to the development of techniques for calculating additional sea ice variables (such as sea ice thickness) from the satellite data.

Glossary

Brightness temperature Unit used to express the intensity of emitted microwave radiation received by the satellite, presented in temperature units (K) following the Rayleigh–Jeans approximation to Planck's law, whereby the radiation emitted from a perfect emitter at microwave wavelengths is proportional to the emitter's physical temperature.

Sea ice concentration Percent areal coverage of sea ice.

Sea ice extent Integrated area of all grid elements with sea ice concentration $\geq 15\%$.

See also

Acoustics, Arctic. Antarctic Circumpolar Current. Arctic Basin Circulation. Bottom Water Formation. Ice–Ocean Interaction. Current Systems in the Southern Ocean. Marine Mammal Migrations and Movement Patterns. Millenial Scale Climate Variability. North Atlantic Oscillation (NAO). Okhotsk Sea Circulation. Polar Ecosystems. Polynyas. Satellite Oceanography, History and Introductory Concepts. Satellite Remote Sensing Microwave Scatterometers. Satellite Remote Sensing SAR. Seabird Migration. Sea Ice: Overview. Sea Ice: Variations in Extent and Thickness. Seals. Weddell Sea Circulation.

Further Reading

Barry RG, Maslanik J, Steffen K *et al*. (1993) Advances in sea-ice research based on remotely sensed passive microwave data. *Oceanography* 6(1): 4–12.

Carsey FD (ed.) (1992) *Microwave Remote Sensing of Sea Ice*. Washington, DC: American Geophysical Union.

Cavalieri DJ, Parkinson CL, Gloersen P, Comiso JC and Zwally HJ (1999) Deriving long-term time series of sea ice cover from satellite passive-microwave multisensor data sets. *Journal of Geophysical Research* 104(C7): 15803–15814.

Gloersen P, Campbell WJ, Cavalieri DJ *et al*. (1992) *Arctic and Antarctic Sea Ice, 1978–1987: Satellite Passive-Microwave Observations and Analysis*. Washington, DC: National Aeronautics and Space Administration.

Gurney RJ, Foster JL and Parkinson CL (eds) (1993) *Atlas of Satellite Observations Related to Global Change*. Cambridge: Cambridge University Press.

Jeffries MO (ed.) (1998) *Antarctic Sea Ice: Physical Processes, Interactions and Variability*. Washington, DC: American Geophysical Union.

Massom R (1991) *Satellite Remote Sensing of Polar Regions: Applications, Limitations and Data Availability*. London: Belhaven Press.

Parkinson CL (1997) *Earth from Above: Using Color-Coded Satellite Images to Examine the Global Environment*. Sausalito, CA: University Science Books.

Parkinson CL (2000) Variability of Arctic sea ice: the view from space, an 18-year record. *Arctic* 53(4): 341–358.

Smith WO Jr and Grebmeier JM (eds) (1995) *Arctic Oceanography: Marginal Ice Zones and Continental Shelves*. Washington, DC: American Geophysical Union.

Ulaby FT, Moore RK and Fung AK (1986) Monitoring sea ice. In: *Microwave Remote Sensing: Active and Passive, Vol. III: From Theory to Applications*, pp. 1478–1521. Dedham, MA: Artech House.

SATELLITE REMOTE SENSING MICROWAVE SCATTEROMETERS

W. J. Plant, Applied Physics Laboratory, University of Washington, Seattle, WA, USA

Introduction

Microwave scatterometers are instruments that transmit low-power pulses of radiation toward the Earth's surface at intermediate incidence angles and measure the intensity of the signals scattered back at the same angles from surface areas a few kilometers on a side. Satellite scatterometers operate continuously and therefore scatter from land and ice as well as the ocean. Useful information is available in the signals from land and ice, but will not be discussed here. This article will concentrate on the primary goal of satellite scatterometers: the measurement of near-surface wind speed and direction over the ocean.

Scatterometers achieve this goal by measuring the intensity, or cross-section, of microwave signals backscattered from the ocean surface. Common frequencies of the transmitted signals for satellite scatterometers are near 5.3 GHz (C-band) on European instruments and 14 GHz (Ku-band) on US ones. At these frequencies, microwaves penetrate only a few millimeters into sea water, so all backscatter originates at the surface and is caused by the roughness of the surface; a perfectly calm sea surface produces no detectable scattering in the direction of the incident radiation. Changes in the average roughness of the ocean surface over scales of several kilometers are caused primarily, but not exclusively, by changes in the wind speed or direction at the ocean surface. Standard assumptions of scatterometry are that the backscatter cross-section, usually called σ_o, over such scales depends only on parameters of the scatterometer and on the mean wind, increases with wind speed, is a maximum when the antenna looks upwind, and is a minimum when the antenna looks

nearly perpendicular to the wind, or crosswind. These assumptions allow the wind speed and direction to be determined from cross-sections measured for the same patch of the ocean, but with the antenna directed at several different azimuth angles. For satellite scatterometry a given patch of ocean can be viewed from several different directions only by allowing the scatterometer to sweep its antenna beams across the patch, a process that requires as much as 4 min. Thus an additional assumption of scatterometry is that average winds over kilometer-scale patches of ocean surface are stationary for several minutes.

With these assumptions and an adequate definition of the wind being measured (discussed below), satellite scatterometers have proven to be able to measure winds over the ocean with accuracies as good as or better than *in situ* measurement techniques. Because oceans cover most of the Earth, this means that microwave scatterometers carried on satellites can monitor the wind field over most of the globe every few days. **Table 1** gives typical specifications that a satellite scatterometer can be expected to meet.

The spatial coverage offered by satellite scatterometry is far better than can be achieved by *in situ* measurements. It allows scatterometers to provide data to study global weather patterns,

Table 1 Expected specifications of the NSCAT satellite scatterometer

Parameter	Value	Accuracy/comment
Wind speed	3–30 m s^{-1}	2 m s^{-1} or 10%
Wind direction	3–30 m s^{-1}	20°
Spatial resolution	50 km	Wind cells
Location accuracy	25/10 km	Absolute/relative
Coverage	90% of ice-free ocean	Every 2 d
Mission duration	3 y	Includes check out

(Data from Naderi *et al.* 1991.)